ISIJ International, Vol. 51 (2011), No. 4, pp. 651–656

Development of Ultrafine Lamellar Ferrite and Austenite Duplex Structure in 0.2C5Mn Steel during ART-annealing

Chang WANG, Jie SHI, Cun Yu WANG, Wei Jun HUI, Mao Qiu WANG, Han DONG and Wen Quan CAO

National Engineering Research Center of Advanced Steel Technology (NERCAST), Central Iron and Steel Research Institute (CISRI), Beijing, 100081 P. R. China.

(*Received on September 7, 2010; accepted on December 22, 2010*)

The microstructural evolution of Fe–0.2C–5Mn steel during intercritical annealing with holding time for up to 144 hours was examined by TEM and STEM. It was demonstrated by TEM that the martensite lath structure gradually transformed into a lamellar ferrite and austenite duplex structure. The partitioning of manganese from ferrite to austenite was found by STEM. Typical Kurdjumov-Sachs orientation relationship between austenite lath and ferrite lath was observed by electron back scattered diffraction (EBSD). Based on the analysis of the austenite lath thckening behavior, it was proposed that the Mn-partitioning in austenite dominated the microstructure evolution of the ultrafine lamellar ferrite and austenite duplex structure during annealing process.

KEY WORDS: austenite reverted transformation (ART); manganese partitioning; ultrafine lamellar duplex structure; Kurdjumov-Sachs orientation relashionship; intercritical annealing.

1. Introduction

Reducing vehicle weight by means of application of high strength and high ductility steel sheet is one of straightforward ways to improve crashworthiness so as to secure the safety of the passengers in the automobile and to improve fuel economy for the sustainable natural energy application.[1] This situation drove the world widely study on the new generation steel with high strength and high ductility.[2]

In light of the excellent ductility of TRIP steel and TWIP steel, it could be expected that increasing the austenite faction with relative stability could increase the ductility effectively. So far, several heat treatment methodologies were demonstrated to be capable of introducing austenite islets into the steel matrix, such as the intercritical annealing followed by bainite holding as applied in TRIP steel fabrication,[5–8] quenching and partitioning (Q&P) to prepare ultrahigh strength steel with relative ductility[9] and austenite reverted transformation from martensite (ART) to produce high strength and high ductility.[10–13] Amongst these methods, ART-annealing was shown to be able to produce large fractioned austenite and ultrafine grain sized structure.[10–13,15,16] However, few reports about the phase transformation behavior and microstructure evolution during ART-annealing were reported in literatures. Specially for the ultrafine grained duplex steel, the measurement of the solution element content and distribution in the matrix and new phase is crucial for us to understand its Partitioned-Local Equilibrium behaviors,[17] which needs to be carried out by scanning transmission electron microscopy (STEM) for its accuracy.[18–20]

In this study, microstructure evolution and solute partitioning behaviors during ART-annealing of Fe–5Mn–0.2C steel were examined through TEM, EBSD and STEM. Our aim is to experimentally study the microstructure evolution behavior of Fe–0.2C–5Mn steel during ART-annealing.

2. Experimental

Fe–0.2C–5Mn steel with 0.2% carbon and 4.72% Mn were prepared by high frequency induction furnace in a vacuum atmosphere. The ingots were homogenized at 1250°C for two hours, forged in between 1200°C–850°C into rods with diameter of ϕ16 mm, and lastly cooled in furnace to room temperature. These forged rods were quenched into oil after austenization at 750°C for half an hour and then ART-annealed at 650°C in electrical box furnace for up to 144 hours and finally air cooled to room temperature.

Microstructure evolution during ART-annealing was carefully examined by transmission electron microscopy (TEM). The orientation relationship between FCC-BCC was analyzed by electron back scattered diffraction in scanning electron microscopy with field emission gun (EBSD-FEG/SEM). Manganese contents in ferrite and austenite were measured by STEM to study the Mn partitioning behaviors from ferrite to newly formed austenite. Thin foils for TEM and EBSD measurements were firstly ground mechanically down to ~40 μm in thickness, and then twin-jet polished in a solution of 5% perchloric acid and 95% alcohol at about –20°C.

3. Results

3.1. Microstructure Evolution during ART-annealing Characterized by TEM

The martensite microstructure of Fe–0.2C–5Mn steel

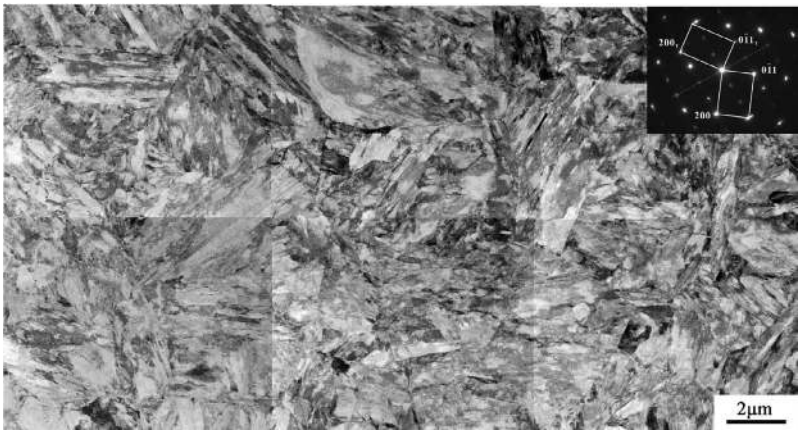

Fig. 1. Microstructure of the oil quenched Fe–0.2C–5Mn after austenization at 750°C with 30 minutes.

quenched in oil after austenization at 750°C with 30 minutes was characterized by TEM (**Fig. 1**). Retained austenite was hardly found in this martensite structure based on the TEM examination. Thus the microstructure after oil quenching is the full martensite structure.

It could be discerned easily that the initial austenite grain size is about 5 μm with three to four α-martensite packets in each prior austenite grain (see in the inserted SAD). Due to the relative high manganese content, a small fraction twined martensite was also found in the quenched state (as indicated by the inserted SAD in Fig. 1). The thickness of the martensitic lath is about 0.1–0.15 μm. High dislocation density could be observed by image contrast (Fig. 1) and was evidenced by the measured dislocation density of $\sim 9\times10^{15}$ m^{-2} from the broadening of X-Ray Diffraction Profiles. In the quenched state, no precipitation could be found in this martensite structure.

In contrast with the high dislocation density, the martensite structure was partially recovered through annihilation of dislocations, coalescence of martensite laths and polygonization of martensite laths after 1 and 5 minutes annealing at 650°C (**Figs. 2**(a), 2(b)). The austenite laths as marked in Figs. 2(a) and 2(b) were identified by selected area diffraction (SAD) in this annealed structure, one is austenite laths developed in between the martensite laths with thickness ~0.1 μm and aspect ratio ~5 (Some are as marked LA), and another is granular austenite grains with size ~0.4 μm located in the prior austenite grain boundary and/or packet boundary in this short time annealed specimens (as marked GA). Due to the recovery and coalescence of martensite, the grain size of the ferrite phase is ~0.4 μm.

After annealing at 650°C for 5 minutes, the martensite structure was highly recovered through annihilation of dislocations (Fig. 2(b)). Rod or granular shaped precipitates of carbides along the original martensitic lath interfaces or some crystallographic faces in the coalescenced martensite laths, which was identified as M_3C as shown by the inserted SAD in Fig. 2(b). STEM analysis indicated that ~20% Mn was included in the carbides. The amount of precipitates is somewhat larger than that in the specimens annealed for 1 minute. Concurrently the laths and the equiaxed grains with parallel stacking faults feature were identified as the reverted austenite by selected area diffraction (SAD). It can be seen clearly from Fig. 2(b) that more lath austenite laths

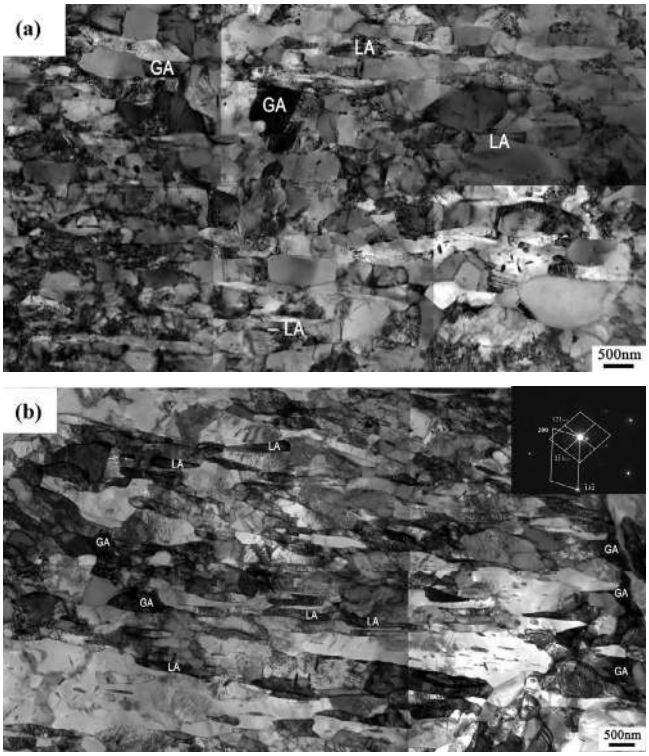

Fig. 2. Microstructure of Fe–0.2C–5Mn ART-annealed for short time at 650°C after austenization at 750°C for 30 minutes and oil quenching (a) 1 minute annealing and (b) 5 minutes annealing.

developed in between the Martensitic laths than that in the specimens annealed for 1 minute whereas the equiaxed austenite grains formed in the Martensitic packet boundary or the original austenite grain boundary. This austenite distribution implies that the austenite prefers nucleating in the martensitic lath interfaces, the packet boundary and the original austenite grain boundary. The thickness of the lath typed austenite is ~0.15 μm with aspect ratio ~5, whereas the grain size of the equiaxed austenite is ~0.5 μm, implying the different shape and size of newly developed austenite due to their different nucleation sites. The thickness of the ferrite laths is ~0.3 μm, slightly smaller than that of the specimens annealed for 1 minute, which may be attributed to the newly developed lath austenite in the highly recovered or coalescenced martensite.

After 1 hour annealing at 650°C, the dark/bright alternative lamellar structure in the original martensitic packets became more clear (**Fig. 3**(a)). Equiaxed austenite grains could be found in the packet boundary or original austenite grain boundary as found in the short time annealed specimens (as shown in Fig. 2). Similar to the specimens annealed for 5 minutes, the needle-like and granular precipitates of M_3C still exist in the coalescenced martensite laths but the amount decreases with elongation of annealing time, indicating its decomposition with increasing annealing time. After 1 hour annealing, the thickness of the austenite laths is ~0.2 μm with aspect ratio larger than 5, and the thickness of ferrite laths is ~0.3 μm. Similar to the BCC-FCC duplex microstructure (as revealed in Fig. 3(a)), parallel band microstructure was found in Fe–0.2C–5Mn steel after 6 hours, 12 hours and 48 hours ART-annealing at 650°C as shown in Figs. 3(b), 3(c) and 3(d). After 6 hours, 12 hours and 48 hours annealing, the austenite thicknesses are ~0.25 μm, ~0.3 μm and ~0.33 μm, respectively, slightly thicker than that of the specimens annealed for 1 hour.

In order to check the thermal stability further, the annealed microstructures of specimens after annealing 144 hours at 650°C were examined by TEM (**Fig. 4**). It was found the average thickness of austenite lath and ferrite lath are ~0.33 μm and ~0.42 μm respectively, and no precipitate could be found in Fig. 4. It can be concluded from these TEM observations that austenite nucleation thickening along the lath boundary were more dominant than that in other sites, such as the prior austenite grain boundary, packet boundary and block boundary during ART-annealing process for Fe–0.2C–5Mn steel. The microstructure of Fe–0.2C–5Mn steel is rather stable during ART-annealing at 650°C. The thicknesses of ferrite lath and austenite lath as a function of annealing time were measured from TEM and summarized in **Table 1**, in which the experimental error was given in the parenthesis to show the spreading of the measured value. It can be seen that both the thicknesses of ferrite lath and austenite lath remain smaller than 0.5 μm even after 144 hours ART-annealing at 650°C.

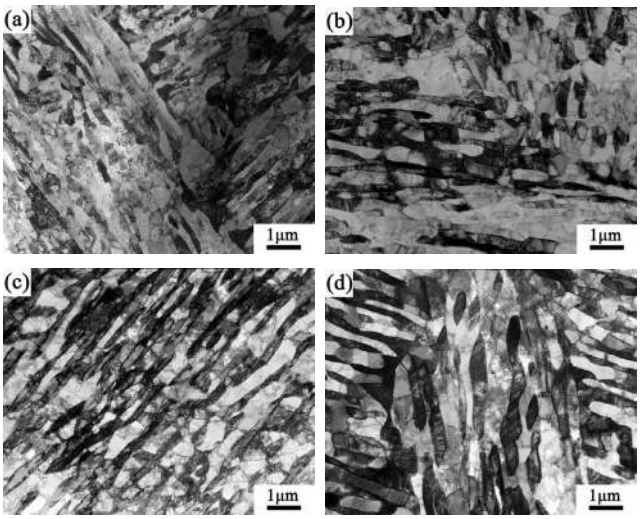

Fig. 3. Microstructure of Fe–0.2C–5Mn steel ART-annealed at 650°C with (a) 1 hour, (b) 6 hours, (c) 12 hours and (d) 48 hours.

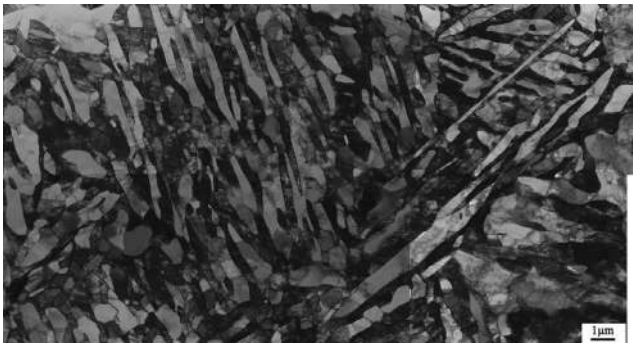

Fig. 4. Microstructures of Fe–0.2C–5Mn ART-annealed at 650°C with ART-annealing for 144 hours.

3.2. Orientation Relationship between Austenite and Ferrite Measured by EBSD

In order to reveal the orientation relationship between austenite and its neighbored martensite laths, the Fe–0.2C–5Mn steel were austenitized at 1250°C to obtain large aus-

Table 1. Apparent thickness ferrite lath and austenite lath measured from TEM (experimental error was given in the parenthesis showing spreading of measured data).

Time	1 minute	5 minutes	1 hour	6 hours	12 hours	48 hours	144 hours
α (μm)	0.4 (0.17)	0.3 (0.1)	0.3 (0.1)	0.3 (0.1)	0.3 (0.1)	0.4 (0.1)	0.4 (0.1)
γ (μm)	0.1 (0.07)	0.15 (0.09)	0.2 (0.1)	0.25 (0.1)	0.3 (0.1)	0.3 (0.1)	0.33 (0.15)

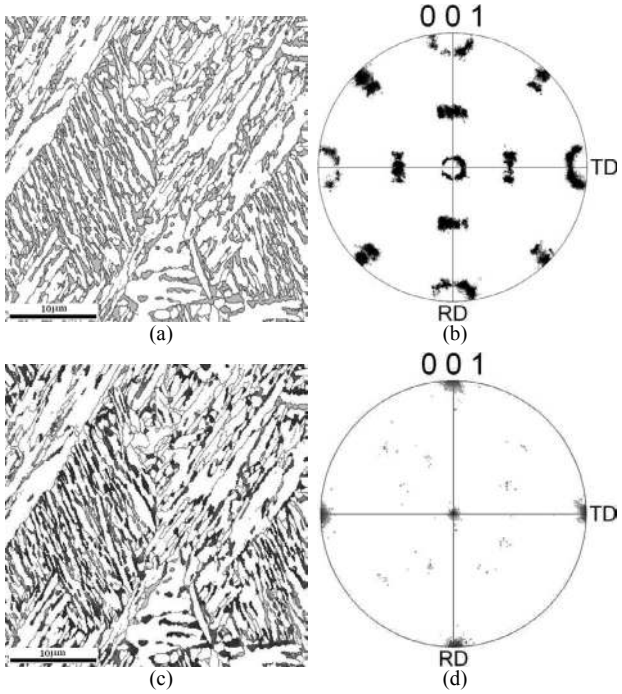

Fig. 5. Microstructure of Fe–0.2C–5Mn steel ART-annealed at 650°C with 6 hours and finally cooled in air after austenisation at 1250°C with 30 minutes and oil quenching (a) Distribution and morphologies of reverted austenite phase colored with green, in which the white part is the ferrite phase, (b) (001) pole figure of BCC phase to reveal the orientation relationship among ferrite laths, which was shown as the white part in (a), (c) orientation deviation of austenite laths from ideal cube orientation, in which the ideal cube orientation was highlighted as blue color, and (d) (001) pole figure to show the orientation distribution of austenite phase, which was highlighted by different colors.

tenite grain size and then ART-annealed at 650°C to develop BCC-FCC duplex structure (**Fig. 5**).

In Fig. 5(a), the austenite was highlighted by green color, and the ferrite was revealed by white color. The low angle boundaries with misorientation between 3–15 deg were depicted by blue color lines and the high angle boundaries over 15 deg were shown by black lines. From Fig. 5(a), it can be seen that only three packets were included in this measured zone and all the austenite laths are nearly parallel to the martensite lath, which further suggested that the austenite mainly developed in the martensite lath interfaces. The typical Kurdjumov-Sachs (K-S) orientation relationship between ferrite laths were plotted in (001) pole figure (Fig. 5(b)), suggesting the inheritance of orientation relationship from the original orientation variants of martensitic laths.[21,22] The orientations deviation from ideal cube orientation of austenite was revealed in Fig. 5(c) with blue color for ideal cube orientation changing to green color and to red color for the orientation away from ideal cube orientation. The corresponding (001) pole figure of austenite was presented to show the orientation deviation of austenite in Fig. 5(d). It can be concluded that most of the austenite laths within different packets in one prior austenite grain assume one orientation, which were reversely transformed from martensite according to K-S orientation relationship. However, it has also been found that some austenite grains located in the packet boundaries or the block boundaries do not follow the K-S relationship (Figs. 5(c) and 5(d)).

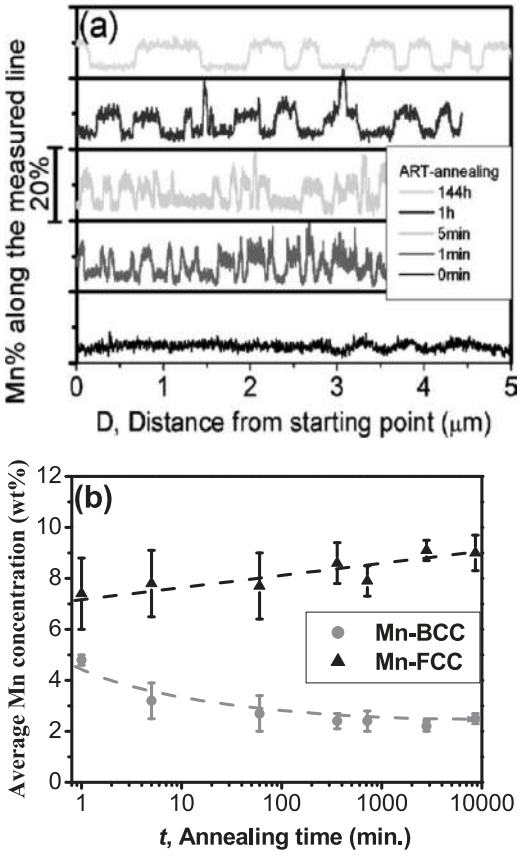

Fig. 6. Profile and Content of Mn measured by STEM (a) Profiles of Mn content along the lines perpendicular to the martensite laths measured by STEM after annealing with different time and (b) The average Mn contents in FCC-lath and BCC-lath measured by STEM as a function of annealing time.

3.3. Phase Identification and Mn Partitioning by STEM

The distribution of Mn contents measured by STEM along the lines perpendicular to the martensite laths were revealed in **Fig. 6**(a) as a function of annealing time. It was identified that the ferrite lath and austenite lath is corresponding to Mn-lean region and Mn-rich region in the Mn content profiles. It can be seen that the apparent austenite peak width of both Mn-lean region and Mn-rich region increases with increasing annealing time. In quenched specimen, the Mn is nearly uniformly distributed in the measured line with an average Mn content ~5.2%(±0.2%), indicating the homogeneous distribution of Mn after quenching. After 1 minute annealing, peaks appeared with Mn% in austenite laths ~7.4%(±1.4%) and in ferrite ~3.2%(±0.7%). With annealing time increasing, the Mn content in austenite increses but that in ferrite decreases gradually, which results in Mn content ~9.0%(±0.7%) in austente and ~2.5%(±0.2%) in ferrite after 144 hours annealing treatment. Mn partition between ferrite and austentie has an influence on the microstructure.[23] The apparent thickness of austenite lath measured based on the peak width and the Mn content in ferrite phase and austenite phase measured by STEM were summarized in **Table 2**.

The Mn concentration profile along the measured lines as shown in Fig. 6(a) indicates the strong Mn partitioning in ferrite and austenite during ART-annealing. The Mn contents in both BCC phase and FCC phase measured by STEM was presented as a function of annealing time as shown in Fig. 6(b). It can be seen from Fig. 6(b) that Mn content slighly increases from 7.4% (±1.4%) in 1 minute annealed specimen to 9% (±0.7%) in 144 hours annealed specimen with increasing annealing time. It is interesting to find that the average Mn content is about 8.1% (±0.7%) in FCC phase and 3.1% (±0.6%) in BCC phase if Mn content was thought not to be affected by annealing time.

4. Discussion

4.1. Microstructure Evolution during ART-annealing and the Underlined Mechanism

Microstructure evolution during ART-annealing

It was revealed by microstructure observation as shown from Figs. 1 to 4 that the microstructure evolved gradually from the full martensite structure to ultrafine ferrite/austenite alternative lath structure with increasing annealing time at 650°C. Two types austenite were clearly observed in the short time annealed specimens (after 1 minute annealing), one is the large equiaxied austenite grain, with grain diameter about 0.4 μm, another is the austenite lath with thickness only about 0.1 μm as shown in Fig. 2(a). The large size

Table 2. STEM measured apparent austenite lath thickness (S_A) and Mn contents in ferrite (Mn_F%) and austenite (Mn_A%) (experimental error was given in the parenthesis showing spreading of measured data).

Time (minute)	0	1	5	60	360	720	2880	8640
S_A (μm)		0.07 (0.02)	0.09 (0.06)	0.18 (0.08)	0.26 (0.15)	0.35 (0.19)	0.30 (0.1)	0.44 (0.1)
Mn_A%		7.4 (1.4)	7.8 (1.3)	7.7 (1.3)	8.6 (0.8)	7.9 (0.6)	9.1 (0.4)	9 (0.7)
Mn_F%	5.2 (0.3)	4.8 (0.2)	3.2 (0.7)	2.7 (0.7)	2.4 (0.3)	2.4 (0.4)	2.4 (0.2)	2.5 (0.2)

of the equiaxed austenite grains after 1 minute annealing implies that its growth is much fast than that of the martensite lath thickening. Also the most of the equiaxed austenite grains were located in the packet or original austenite boundaries. This means that the phase transformation is dominated by the nucleation and growth of the equiaxed austenite grains in the packet and/or prior austenite grain boundaries during very short annealing time. However after annealing for 5 minutes and further elongated annealing time at 650°C, large amount of austenite laths were developed in between the martensite laths (as shown in Figs. 2(b), 3 and 4). Thus the corresponding microstructure was dominated mainly by the ultrafine austenite lath and ferrite lath alternative structure. This ultrafine austenite/ferrite duplex structure means that the nucleation and thickening of lath-typed austenite controlled the phase transformation during long time annealing. In addition, after long time annealing, no precipitations could be found in the microstructure as shown in Fig. 4, which implies that the carbides precipitated in the heating process or in the earlier annealing stage decomposed during long time annealing. Based on above analysis, it can be concluded that the evolution of austenite during annealing process at 650°C could be divided into three stages: (i) austenite nucleation and growth in the prior austenite grain boundary and packet boundary after short time annealing (Fig. 2); (ii) austenite nucleation and growth in between the martensitic lath after relative long time annealing (>5 minutes)(Fig. 3); and (iii) no or slight coarsening, coalescence and breaking of the lath typed austenite grains (Fig. 4). It should be pointed out here that the fraction of the austenite nucleated in boundary regions is significantly lower than that nucleated in between martensitic laths, suggesting that the phase transformation during annealing was mainly controlled by the austenite nucleation and growth in between the martensitic laths.

Orientation relationship and Mn partitioning between ferrite and austenite

The orientation relationship between the ferrite laths as given in Fig. 5(b) obeys the K-S orientation exactly as shown in Fig. 5(b), which clearly indicates that the examined area belongs to one prior austenite grain. Thus it can be concluded that no ferrite laths with new orientation were formed during annealing process. All the orientations of the ferrite laths after annealing were inherited from those of the martensite laths, which follows the K-S relationship. The orientation relationship between the austenite lath and the ferrite lath as shown in Figs. 5(b) and 5(d) was mainly dominated by the K-S relation as well. This means that the phase transformation from martensite to austenite during annealing process at 650°C was mainly controlled by austenite reverted transformation (ART) as demonstrated in literature.[10–13] That is the reason why the annealing at 650°C was simply called ART-annealing for 0.2C5Mn steel in this study. It may be pointed out here, there are still some grains with orientations deviated from the ideal orientation significantly, which may caused by the nucleation and growth of equiaxed austenite grains in the packet boundary as shown in Fig. 2, but this needs to be proved in further study. During ART-annealing process, the Mn contents are about 9% (±0.7%) in austenite and 2.5% (±0.2%) in the ferrite after a long time annealing, which agrees very well with reported data.[24,25] The big difference between the average Mn concentration and that both in austenite lath and ferrite lath indicates there is a strong partition of Mn between two phases during annealing process. In addition, it was well know that the carbon can partition from the bainite phase into austenite at about 400°C during short time bainite holding in TRIP steel. Thus it could be expected that the carbon partition and the Mn partition take place simultaneously during ART-annealing process, which needs further discussion of the effects of C/Mn partitioning on the phase transformation.

4.2. Thickening Behavior of Austenite Lath

The phase transformation of 0.2C5Mn steel obeys the K-S orientation relationship between new developed austenite and the ferrite. During ART-annealing process, this phase transformation mainly takes place by the austenite lath thickening controlled by Mn or C partitioning. It is well know that the thickening behavior of austenite laths can be described by Eq. (1), which usually was applied to describe the thickening of precipitation controlled by solute bulk diffusion,[26]

$$S_A = \lambda\sqrt{Dt} \quad \text{..... (1)}$$

where S_A is the average lath thickness of the newly developed phase, D is the diffusion coefficient, t is the diffusion time and λ is the constant determined by the element content in the new developed phase (X^N),the mother phase(X^M)and its average content(X^0),which could be formulated as (Eq. (2)),[26]

$$\lambda = \frac{4(X^N - X^0)}{\pi^{0.5}(X^0 - X^M)} \quad \text{..... (2)}$$

The thickening slope ($\lambda\sqrt{D}$) of austenite lath could be calculated upon the assumption that the thickening was controlled by carbon bulk diffusion in ferrite and in austenite, or Mn bulk diffusion in ferrite or in austenite, separately. The calculated results and related diffusion data were given in **Table 3**. The austenite lath thickness measured by STEM as recorded in Table 1 were re-plotted as a function of the square root of annealing time in **Fig. 7**, which gives a slope of about 0.00426 μm/minute$^{0.5}$. It can be seen that the experimental results agree very well with the calculated slope based on the Mn diffusion in austenite, suggesting the austenite thickening behaviors is controlled by Mn diffusion in austenite. Thus the high thermal stability of the ultrafine grained duplex microstructure of Fe–0.2C–5Mn steel at 650°C was attributed to the slow diffusion rate of Mn in austenite. However, it may be argued that the slope as indicated in Fig. 7 is slightly higher during short annealing period (annealing time less than 6 hours) than the average fitted

Table 3. Theoretically calculated results of the austenite lath thickening slope ($\lambda\sqrt{D}$).

Diffusion type	Element content	λ	Diffusion coefficient (D, cm^{2}s^{-1})	$\lambda\sqrt{D}$ (μm/minute$^{0.5}$)
***C* in Ferrite**	0.02%	5	0.0062exp(–80000/RT)[27]	165.7
***C* in Austenite**	0.57%	5	0.1exp(–13000/RT)[27]	17.28
***Mn* in Ferrite**	2.5%	3.6	0.35exp(–220000/RT)[27]	0.0975
***Mn* in Austenite**	9.0%	3.6	0.16exp(–261000/RT)[27]	0.00455

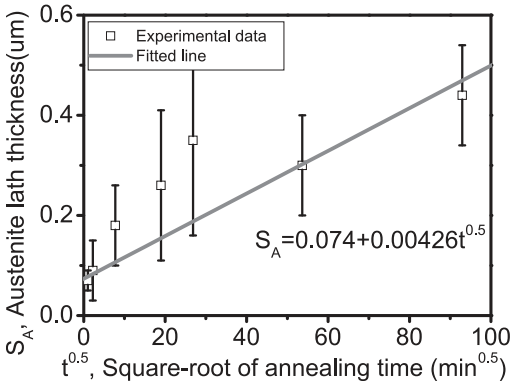

Fig. 7. Comparison of the austenite thickening behavior measured by STEM and that calculated from Eq. (1) based on Mn diffusion in austenite and ferrite, respectively.

slope, which may be ascribed by following two possible reasons. One is that the thickening of the austenite lath involves not only the Mn partitioning but also the C partitioning, thus the thickening cannot be exactly predicted by Mn partition. Because of the fast partitioning of C, it definitely enhances the thickening of the austenite lath in the annealing period with short time. And another reason is that some of the thin austenite laths may not be measured by TEM due to the difficulty to measure the very thin austenite lath, which results in a high average value of the thickness of austenite laths and in turn a slightly higher slope in the short annealing time period.

Based on the discussion above, it could be concluded that the increasing of austenite volume fraction was developed mainly by austenite lath thickening in between neighbored martensite laths. During annealing process, the thickening of the austenite lath is mainly controlled by Mn diffusion in austenite phase, which was confirmed by the theoretical calculation.

5. Conclusion

The development of ultrafine lamellar ferrite and austenite duplex structure of Fe–0.2C–5Mn steel during ART-annealing process was studied at 650°C with annealing time for up to 144 hours. The main conclusions could be summarized as follows,

(1) ART-annealing of Fe–0.2C–5Mn steel resulted in the microstructure evolution from fully martensite structure to an ultrafine lamellar ferrite and austenite duplex microstructure. Significant difference of Mn concentrations between ferrite lath and austenite lath were found by STEM, which indicates a strong Mn partitioning during ART-annealing process.

(2) The growth behavior of austenite is carried out by austenite lath thickening, *i.e.*, one dimension growth along thickness direction, which could be described by the linear relation between average lath thickness and the square-root of annealing time, $S_A = \lambda\sqrt{Dt}$. The thickening of austenite lath was controlled by Mn diffusion in austenite phase.

(3) Even after 144 hours annealing at 650°C, the thickness of both austenite lath and ferrite lath remains smaller than 0.5 μm, indicating the high thermal stability of the ultrafine grained duplex microstructure of Fe–0.2C–5Mn steel, which may be attributed to the slow diffusion rate of Mn in austenite.

Acknowledgement

This research is supported by National Basic Research Program of China (973 program) No.2010CB630803 and National High-tech R&D Programs (863 programs) No.2009AA03Z519 and No.2009AA033401.

REFERENCES

1) K. Sugimoto, T. Iida, J. Sakaguchi and T. Kashima: *ISIJ Int.*, **40** (2000), 902.
2) R. Heimbuch, Overview: Auto/Steel partnership, www.a-sp.org
3) C. Garcia-Mateo and F. G. Caballero: *ISIJ Int.*, **45** (2005), 1736.
4) G. Frommeyer, U. Brux and P. Neumann: *ISIJ Int.*, **43** (2003), 438.
5) B. C. De Cooman: *Curent Opinion in Solid State & Mater. Sci.*, **8** (2004), 285.
6) P. Jacques, Q. Furnemont, A. Mertens and F. Delannay: *Philos. Mag. A*, **81** (2001), 1789.
7) E. Girault, A. Martens, P. Jacques, Y. Houbaert, B. Verlinden and J. VanHumbeeck: *Scr. Mater.*, **44** (2001), 885.
8) E. V. Pereloma, I. B. Timokhina and P. D. Hodgson: *Mater. Sci. Eng.*, **A273–275** (1999), 448.
9) C. Y. Wang, J. Shi, W. Q. Cao and H. Dong: *Mater. Sci. Eng.*, **A527** (2010), 3442.
10) R. L. Miller: *Metall. Trans.*, **3** (1972), 905.
11) K. T. Park, E. G. Lee and C. S. Lee: *ISIJ Int.*, **47** (2007), 294.
12) N. Nakada, T. Tsuchiyama, S. Takaki and S. Hashizume: *ISIJ Int.*, **47** (2007), 1527.
13) T. Hara, N. Maruyama, Y. Shinohara, H. Asahi, G. Shigesato, M. Sugiyama and T. Koseki: *ISIJ Int.*, **49** (2009), 1792.
14) H. S. Zurob, C. R. Hutchinson, Y. Brechet, H. Seyedrezai and G. R. Purdy: *Acta Mater.*, **57** (2009), 2781.
15) M. Niikura and J. W. Morris, Jr.: *Metall. Trans. A*, **11A** (1980), 1531.
16) H. N. Han, C. S. Oh, G. Kim and O. Kwon: *Mater. Sci. Eng.*, **A499** (2009), 462.
17) M. Enomoto and H. I. Aaronson: *Metall. Trans. A*, **18A** (1987) 1547.
18) H. A. Fletcher, A. J. Garratt-Reed, H. I. Aaronson, G. R. Purdy, W. T. Reynolds and G. D. W. Smith: *Scr. Mater.*, **45** (2001), 561.
19) R. E. Hackenberg and G. J. Shiflet: *Acta Mater.*, **51** (2003), 2131.
20) E. S. Humphreys, H. A. Flectcher, J. D. Hutchins, A. J. Garratt-Reed, W. T. Reynolds, H. I. Aaronson, G. R. Purdy and G. D. W. Smith: *Metall. Mater. Trans. A*, **35A** (2004), 1223.
21) S. Morito, H. Tanaka and R. Konishi: *Acta Mater.*, **51** (2003), 1789.
22) H. Kitahara, R. Ueji and M. Ueda: *Mater. Charact.*, **54** (2005), 378.
23) D. W. Suh, S. J. Park and S. J. Kim: *Metall. Mater. Trans. A*, **39A** (2008), 2015.
24) M. Hillert, T. Wada and H. Wada: *J. Iron Steel Inst*, **205** (1967), 539.
25) J. Lis and A. Lis: *J. Achievements Mater. Manuf. Eng.,* **26** (2008), 195.
26) H. I. Aaronson, C. Laird and K. R. Kinsman: Phase transformations, ASM, Ohio, (1968), 313.
27) E. A. Brandes: Smithells Metals Reference Book(B). 6th Ed., Butterworths, London, (1983).